Journal of Power Sources 195 (2010) 7054–7060

Contents lists available at ScienceDirect

Journal of Power Sources

journal homepage: www.elsevier.com/locate/jpowsour

Layer by layer assembly of hybrid nanoparticle coatings for proton exchange membrane fuel cell bipolar plates

Feng Wang[a], Mubarak Alazemi[a], Indrajit Dutta[a,1], Richard H. Blunk[b], Anastasios P. Angelopoulos[a,*]

[a] Chemical and Materials Engineering Department, University of Cincinnati, 400 Rhodes Hall, Cincinnati, OH 45227, United States
[b] Electrochemical Energy Research Laboratory, General Motors Corporation, 30500 Mound Rd., Warren, MI 48090, United States

ARTICLE INFO

Article history:
Received 13 March 2010
Received in revised form 6 May 2010
Accepted 7 May 2010
Available online 31 May 2010

Keywords:
Bipolar plates
Nanotechnology
Layer by layer assembly
Thin films
Coatings

ABSTRACT

Optimum proton exchange membrane (PEM) fuel cell operation at low reactant gas stoichiometry requires that bipolar plate surfaces combine negligible electrical contact resistance with a high degree of hydrophilicity. Unfortunately, no single material can simultaneously satisfy both requirements. In the present work, we demonstrate that electrostatic layer by layer (LBL) assembly may be employed to design hybrid coating architectures composed of 5–10 nm thick graphite platelets and 19 nm diameter silica nanospheres. The strong cationic polyelectrolyte, acrylamide/β-methacryl-oxyethyl-trimethyl-ammonium copolymer, is used to deposit the two anionic nanoparticles from both discrete and mixed aqueous suspensions onto gold substrates. Low contact resistance is achieved by maintaining connectivity of the graphite nanoparticles throughout the coating thickness while good hydrophilicity is achieved by controlling graphite surface domain size. For ~100 nm thick coatings, contact resistances as low as ~4 mΩ cm^2 may be obtained (comparable to that of a pure graphite platelet coating) while maintaining an advancing contact angle of ~20° (comparable to that of a pure silica nanoparticle coating). This result represents an order of magnitude reduction in ohmic power loss for state-of-the-art PEM fuel cells relative to the use of pure silica nanoparticle coatings. While LBL assembly is a well-established technique for producing thin, layered structures of nanoparticles and polyelectrolytes, this work provides a unique architectural methodology by which domain distribution in heterogeneous nanoparticle coatings may be controlled.

© 2010 Elsevier B.V. All rights reserved.

1. Introduction

The surface wettability and contact resistance of bipolar plate materials significantly impact the operational efficiency of low temperature proton exchange membrane (PEM) fuel cells. Hydrophobic channel surfaces contribute to flow instabilities that increase the pressure drop and parasitic power losses required to maintain reactant gas stoichiometry [1,2]. High contact resistance contributes to increased thermal energy at the expense of useful electrical energy. Independent control over these two critical properties is difficult to achieve using any single material. For example, graphite-epoxy composites as well as gold-, graphite-, or titanium nitride-coated stainless steel materials presently employed for bipolar plates in the fuel cell industry [3] have contact resistances below 20 mΩ cm^2 but advancing water contact angles that exceed 80°. Surfaces with advancing water contact angles as low as 20° have been found necessary for optimum performance [4,5] and have been obtained with stable silica coatings as thin as 63 nm but with a contact resistance of 17 mΩ cm^2 greater than that of the base substrate [5,6]. For a 400 cell state-of-the-art PEM fuel cell stack with a 300 cm^2 active area operating at 1 A cm^{-2}, even such a seemingly low coating contact resistance contributes an additional 2 kW ohmic power loss [7].

In the present work, we investigate whether electrostatic layer by layer (LBL) assembly may be employed to create hybrid bipolar plate coatings composed of both electrically conductive graphite platelets and hydrophilic silica nanoparticles to maximize PEM fuel cell efficiency. LBL assembly is a well-established technique for producing thin, layered structures of nanoparticles and polyelectrolytes in a very cost-effective manner [8,9]. However, control over surface domain distribution, a key factor affecting surface wetting behavior [10–14], is uncertain.

LBL assembly of graphite platelets was previously shown to yield coatings with very low electrical contact resistance (below 4 mΩ cm^2) [15]. Graphite suspension stabilization and electrostatic assembly were achieved through hydrolysis to yield carboxylic acid functional groups (approximately 5% of the total surface carbons) which dissociate at sufficiently high suspension pH to yield a neg-

* Corresponding author. Tel.: +1 513 556 2777; fax: +1 513 556 3443.
E-mail address: anastasios.angelopoulos@uc.edu (A.P. Angelopoulos).
[1] Present address: General Motors Corporation, 30500 Mound Rd., Warren, MI 48090, United States.

0378-7753/$ – see front matter © 2010 Elsevier B.V. All rights reserved.
doi:10.1016/j.jpowsour.2010.05.014

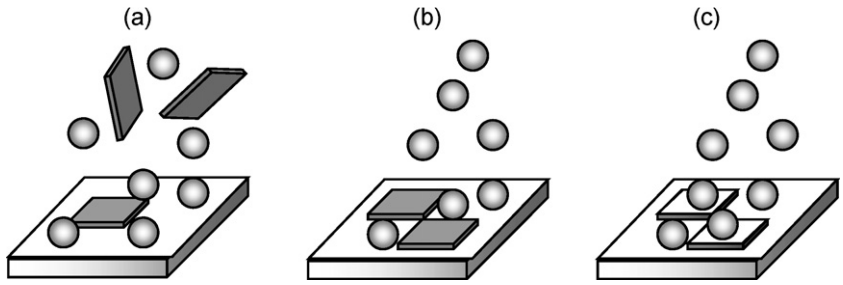

Fig. 1. Schematic of nanoparticle architectures investigated in this article: (a) cLBL assembly, (b) dLBL assembly, and (c) sLBL assembly. Only the end of the initial process cycle (substrate immersed in final suspension and prior to rinsing) is shown. Graphite platelets are depicted by shaded rectangles and shown in mixed suspension with silica nanoparticles (open circles) as in scheme (a) or adsorbed onto the white cationic polyacrylamide-coated substrate surface as in schemes (a) through (c). An intervening cationic polyacrylamide immersion during each process cycle of sLBL assembly also deposits the polyelectrolyte onto the graphite platelets, as is shown in scheme (c). For all three schemes, the silica nanoparticles are found in suspension as well as adsorbed on the cationic polyacrylamide.

ative charge. Such functionality was found to yield coatings with an average advancing water contact angle of 60° with a standard deviation of 7°, depending on process conditions. In this work, we augment the hydrophilicity of these graphite coatings by systematically introducing silica nanoparticles into their structure. Unlike previous studies involving electrostatic LBL assembly of nanoparticles with complementary charges [16–18], the nanoparticles employed in the present investigation are all negatively charged. In the case of silica, this charge arises from dissociation of silanol groups [6]. Consequently, the use of a cationic binder is required to produce the desired hybrid coatings. Whereas LBL assembly has been previously employed to combine the functionality of more than two types of polyelectrolytes [19], specific approaches for producing well-defined composite structures of polyelectrolytes and chemically heterogeneous nanoparticles via electrostatic LBL assembly are not available. Electrostatic repulsion between similarly charged nanoparticles opens up the possibility of creating unique three-dimensional architectures not previously observed. Three coating architectures are explored in the present investigation and are diagramed schematically in Fig. 1. The shaded rectangles in Fig. 1 indicate the anionic graphite platelets while the open circles indicate the anionic silica nanoparticles, not drawn to scale. Both nanoparticles in suspension as well as adsorbed on the substrate surface are shown. The pre-adsorbed cationic polyelectrolyte is designated as a white plane on the surface of the substrate in Fig. 1(a) and (b) and, in the case of Fig. 1(c), on the surface of the graphite platelets as well. The specific features of each architecture are as follows:

Scheme 1, Fig. 1(a). Competitive LBL (cLBL) assembly involves the simultaneous application of graphite and silica onto a cationic polyelectrolyte layer from mixed suspension. Self-assembled monolayers (SAMs) of mixed alkanethiol molecules [20] as well as LBL assembly of polyelectrolyte blends [19] are well known. However, it is uncertain whether the order of magnitude differences in adsorption kinetics that have been previously observed between different types of nanoparticles [6,15] will produce complete screening of available surface sites by one type of nanoparticle or whether a heterogeneous nanoparticle domain structure will form.

Scheme 2, Fig. 1(b). Directed LBL (dLBL) assembly involves the application graphite and silica onto a cationic polyelectrolyte layer from discrete suspensions. Previous LBL investigations have routinely shown that complete coverage of the substrate surface is seldom achieved after the deposition of a single bilayer of two complementary polyelectrolytes [21–25] or a polyelectrolyte binder and nanoparticles [15]. Instead, the initial bilayer adsorbs in the form of islands which grow and coalesce with the application of additional bilayers [15,22]. During dLBL assembly, we use each porous bilayer of graphite platelets adsorbed onto cationic polyelectrolyte to direct the subsequent deposition of silica nanoparticles away from the graphite surfaces and onto available interstitial sites containing cationic polyelectrolyte. The probability of direct graphite platelet contact between adjacent layers is thus substantially enhanced relative to Scheme 1 and may lead to more electrically conductive coatings.

Scheme 3, Fig. 1(c). Standard LBL (sLBL) assembly involves the application of graphite and silica from discrete suspensions with an intervening cationic polyelectrolyte layer. This intervening layer is anticipated to reverse the charge of the previously adsorbed carbon nanoplatelets and permits adsorption of the silica directly onto their surface, unlike the repulsive interaction and domain separation that likely occur between the two types nanoparticles in either the cLBL or dLBL assembly schemes. For this final scheme, we will investigate whether the porosity of both the silica nanoparticles and the polyelectrolyte permits sufficient contact between alternating graphite layers to yield electrically conductive coatings. The role of surface domain separation on multilayer coating wettability will be examined for all three architectures.

2. Materials and methods

2.1. Materials

The raw materials employed for making pure and mixed nanoparticle suspensions consisted of Aqudag E graphite paste, X-TEC 3408 silica nanoparticle suspension (NanoX Corporation), H_2SO_4 (ACS Plus Grade, Fisher Scientific), ethanol (Fischer Scientific, ACS Spectrophotometric Grade), and de-ionized (DI) water obtained by passing a 1 MΩ resistivity house water supply through a Millipore Synthesis water purification unit to achieve 18.2 MΩ. The graphite platelets and silica nanoparticles have previously been extensively characterized [6,15]. In summary, the graphite platelets are composed of stacked graphene sheets having a total thickness of between 5 and 10 nm. The graphite platelets have high polydispersity, with the flat dimension ranging from 0.2 to 1.7 μm. The silica nanoparticles are spherical, with an average diameter of 19 nm and polydispersity of 0.29 obtained from photon correlation spectroscopy measurements.

Preparation of the pure nanoparticle suspensions follows the procedures previously published in the literature [6,15]. The pH of both suspensions was maintained at a value of 5 using H_2SO_4. This value was found to be sufficiently high to ensure suspension stability yet sufficiently low to prevent dissociation of hydrolyzed groups on the cationic binder employed for LBL assembly. Alcohol-free media was employed for the graphite suspension, yielding a zeta (ζ) potential of −38 mV. Ethanol (50 vol%) was added to the

pure silica suspension, yielding a ζ potential of −37 mV. The suspensions consisted of 5 wt% graphite (carbon) and 0.5 wt% silica. Mixed nanoparticle suspensions were prepared utilizing the same pH and concentrations as the pure suspensions. Negligible change was observed in pure nanoparticle ζ potentials under mixed suspension conditions. Photon correlation spectroscopy analysis and pH measurement and adjustment of the suspensions were performed intermittently to ensure stability.

Electroplated gold of 20 nm thickness on 316-L stainless steel was employed as the substrate material for LBL assembly. This material is one of the numerous types presently under consideration for bipolar plates in PEM fuel cell applications. Samples consisted of 2.54 cm × 2.54 cm squares wiped clean with ethanol immediately prior to LBL assembly.

The polyelectrolyte, acrylamide/β-methacryl-oxyethyl-trimethyl-ammonium copolymer, was employed as the cationic polymer binder for LBL assembly. The material has previously been extensively characterized [6,15,21,25] and found to have a ζ potential ranging form 7 mV at pH 1 to 29 mV at pH 5. Both pH values (adjusted using H_2SO_4) were employed for cLBL assembly while only a pH value of 5 was employed for dLBL and sLBL assemblies. The cLBL assembly scheme consisted of initial sample immersion to the cationic polymer solution for 2 min for adsorption equilibration followed by thorough rinsing in DI water (two 1-min increments into first a dirty then clean rinse). The sample was then immersed into the mixed nanoparticle suspension for 10 min to ensure equilibration based on previous investigations [6,15] and then thoroughly rinsed. This consisted of a single application cycle. Additional layers were applied by repeating this cycle without intermediate drying. The final coating was allowed to dry overnight at ambient temperature prior to characterization. The dLBL assembly scheme consisted of initial immersion of a sample into the cationic polymer for 2 min, followed by a 2-min cumulative rinse time in DI water, 10-min immersion in pure graphite suspension, another 2 min of cumulative DI water rinsing, immersion into a pure silica suspension for 2 min for adsorption equilibration, and a final 2-min cumulative DI water rinse. The entire sequence was considered a single application cycle and repeated to form multilayer coatings. Coating was dried as described previously. The sLBL assembly scheme was identical to dLBL with the exception that a cationic polymer application step was inserted between the graphite rinse and the silica deposition. This step consisted of 2-min immersion into the cationic polymer solution followed by a 2-min cumulative DI water rinse. Vigorous manual agitation was employed during rinsing of the samples whereas no agitation was employed while the samples were immersed in the polymer solution and nanoparticle suspensions.

2.2. Characterization

The instrumental methods employed in the present investigation have been described in detail elsewhere [6,15] and are only briefly summarized here. PCS (Zeta-Plus from Brookhaven Instruments) was employed for particle size and ζ potential measurement. High resolution secondary electron (SEM) images of the deposited surface layers were obtained using a Carl Zeiss NVision 40 Crossbeam® workstation with a LEO Gemini® field emission column. The column is provided with an "in-lens" annular secondary electron (SE) detector. A beam energy of 3 kV and WD of ∼3.5 mm were used. An FEI XL-30 System SEM equipped with an energy dispersive X-ray spectrometer (EDS, EDAX Corp.), was employed to monitor changes in the elemental composition of the LBL coatings. Semi-quantitative analysis was performed at a constant accelerating potential of 15 keV, a working distance of 10 mm, an amp time of 51.2 μs and a magnification of 200×. The C, O, and Si K emission intensities were compared to the Au L emission intensity for relative analysis with results reported as wt%. AFM images were obtained using a Dimension 3100 (Veeco Metrology Group) operated in constant force mode. Best images were obtained utilizing a tip with a nominal radius of 20 nm (DNP, Veeco) and an image area of 20 μm × 20 μm. Dynamic contact angle measurements were made utilizing a Sigma 701 wetting balance (KSV). (A minimum of three immersion cycles was performed to ensure reproducibility with the standard deviation indicated by the error bars in the figures of this paper.)

Electrical contact resistance was assessed using a custom built apparatus based on a Carver hand-press. Gold coated platens were attached to swivel points on the press and connected to a power supply. Teflon tape on one platen surface defined a 6.45 cm^2 contact area into which was placed a 6.45 cm^2 coated sample. The sample was first sandwiched between two conductive compliant sheets of graphite fiber paper (Toray TGP-H-1.0T) to permit the controlled application of a contact pressure of 1379 kPa for all measurements. The through-plane potential drop at an applied current density of 1 A cm^{-2} (6.5 A) was read which, when subtracted by the potential drop for the bare substrate and divided by two (the sample being coated on both sides), gave the coating contact resistance, R_c, in units of Ω cm^2. In other words: $R_c = RA$ where, R is the through-plane resistance of the coating and A is the contact area perpendicular to the direction of current flow.

The thickness for a given coating was obtained from EDS data using Monte-Carlo electron flight simulations (CASINO Version 2.42, Universite de Sherbrook, Quebec) under the same microscope conditions as discussed above [26]. Results from such simulations yield the k-ratio (the ratio between X-ray intensities from a pure carbon or pure silica coating on pure gold relative to that of a pure carbon or silica substrate, $I_i/I_{i,ref}$, where i is either C or SiO_2) versus the pure component thickness, t_i. We have previously determined that the following relation holds for t_C out to 700 nm [15]:

$$t_C = 1180.8\,\text{nm}\frac{I_C}{I_{C,ref}} \tag{1}$$

and the following relation holds for t_{SiO_2} out to 1000 nm [6]:

$$t_{SiO_2} = 1508\,\text{nm}\frac{I_{SiO_2}}{I_{SiO_2,ref}} \tag{2}$$

The overall coating thickness, t, may then be obtained utilizing [26]:

$$\rho t = \rho_C t_C + \rho_{SiO_2} t_{SiO_2} \tag{3}$$

where ρ is the coating thickness density (calculated from EDS wt% data) and ρ_i is the density for pure component i. Incorporation of adventitious carbon and oxygen on the substrate into the Monte-Carlo simulations is found to have negligible impact on the final coating thickness result. Data reported in this paper were obtained from the average of three measurements on each side of every sample, with the standard deviation indicated by the error bars in the figures. The polymer layer contributes negligibly to the thickness obtained using Eq. (3) as the presence of nitrogen (an element unique to the polymer) cannot be detected in the EDS spectra. Previous analysis of angle-resolved XPS data has indicated that the polymer adsorbs in a flat, all train conformation under similar experimental conditions [21,25].

3. Results and discussion

3.1. Effect of architectural LBL assembly on coating structure

Fig. 2 depicts the variation in coating thickness with the number of assembly "cycles", where each cycle represents the single application of graphite and silica nanoparticles onto a cationic polyacrylamide layer, with or without the presence of an intervening

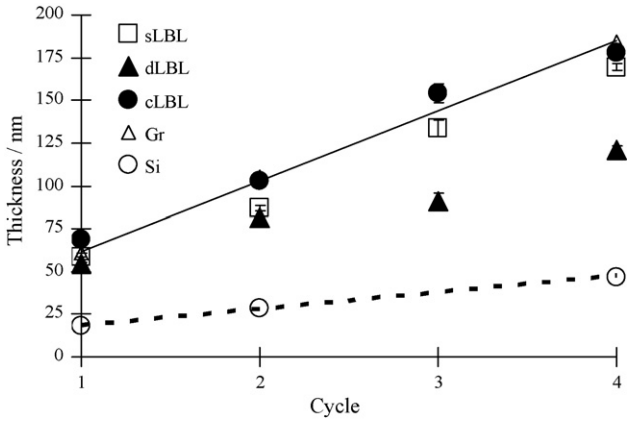

Fig. 2. Coating thickness obtained from the cLBL, dLBL, and sLBL assembly schemes in comparison to that obtained from pure silica nanoparticles (Si) and pure graphite platelets (Gr). Each cycle represents a single graphite-silica nanoparticle application onto cationic polyacrylamide, with (as in the case of sLBL assembly) or without (as in the case of cLBL and dLBL assemblies) an intervening cationic polyacrylamide layer. The solid and dashed lines represent linear fits through the average of previous data obtained with pure Gr and Si, respectively.

cationic polyacrylamide layer (i.e., the latter in the case of sLBL assembly). We note that all architectures exhibit a roughly linear increase in thickness at this initial stage with the number of application cycles and an overall thickness which is much greater than would be expected on the basis of the silica nanoparticle diameter or graphite platelet thickness alone. Such behavior was previously shown to result from clustering of the graphite platelets onto the bare substrate surface [15]. The solid and dashed lines in Fig. 2 represent linear fits through the average of previous data obtained with pure graphite [15] and silica [6], respectively, using the same cationic polyacrylamide as in the present study.

Graphite platelet clustering is observed in scanning electron microscopy (SEM) images of the coating surfaces obtained after a single assembly cycle of each architecture type and shown in Fig. 3. We note from these images that, in the case of cLBL and dLBL assemblies (Fig. 3(b) and (c), respectively), there is clear separation of the graphite and silica domains on the surface due to electrostatic repulsion between the two types of nanoparticles versus the bare gold substrate surface shown in Fig. 3(a). By contrast, the SEM image of the sLBL assembly scheme (Fig. 3(d)) indicates that the intervening cationic polyacrylamide layer permits deposition of silica directly onto the graphite surface. The dispersion of graphite platelets after a single cycle of dLBL and sLBL assemblies is identical to that initially observed with graphite platelets alone (Fig. 8(b) in Ref. [15]), consistent with the use of discrete nanoparticle suspensions and demonstrating the durability of each nanoparticle layer with subsequent suspension immersion. The more highly dispersed graphite platelets observed in Fig. 3(b) for cLBL assembly indicate that competitive adsorption favors silica, consistent with its more rapid adsorption kinetics [6,15].

SEM images of the various architectures after the application of three cycles are shown in Fig. 4. As identified by the white circle in Fig. 4(a), the top layer of cLBL assembled coatings continues to possess graphite platelets completely free of silica while, as shown in Fig. 4(c), that of sLBL assembled coatings is nearly completely covered by silica nanoparticles. Exposed graphite domains at the topmost layer are also identified by a white circle in Fig. 4(b) for the case of dLBL assembly. However, in the case of dLBL assembly, areas where only silica is present on the substrate are also evident and domain separation appears to persist through the coating thickness. In contrast, in the case of both cLBL and sLBL assemblies, nearly the entire substrate surface is coated by graphite platelets after three cycles. Interestingly, despite the competition for surface sites which occurs during cLBL assembly due to repulsive nanoparticle interactions, graphite adsorption from mixed suspension appears to overall yield a more random adsorption pattern than that associated with dLBL assembly.

The morphological information provided by the SEM images in Figs. 3 and 4 clarify the differences in thickness dependence on number cycles shown in Fig. 2 for the three architectures. The thinnest coatings were obtained from dLBL assembly, for which

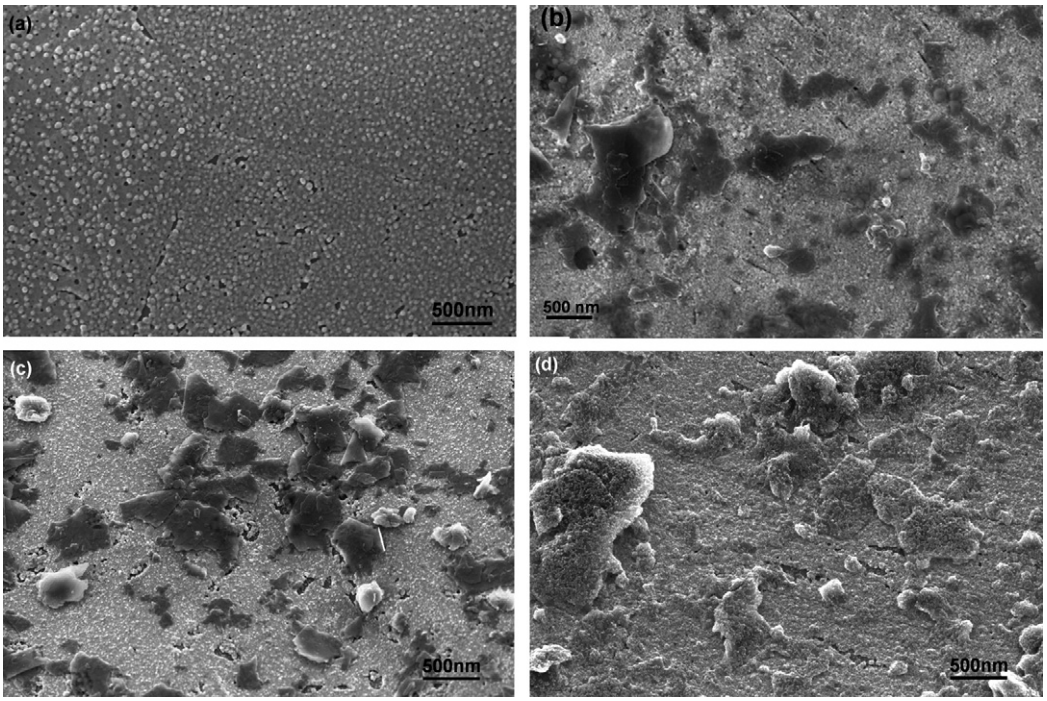

Fig. 3. SEM images at 20–25k× of the surfaces of (a) bare substrate and nanoparticle coatings after the initial process cycle (as shown in Fig. 1) during (b) cLBL assembly, (c) dLBL assembly, and (d) sLBL assembly. Graphite nanoplatelets appear as dark flakes in these images.

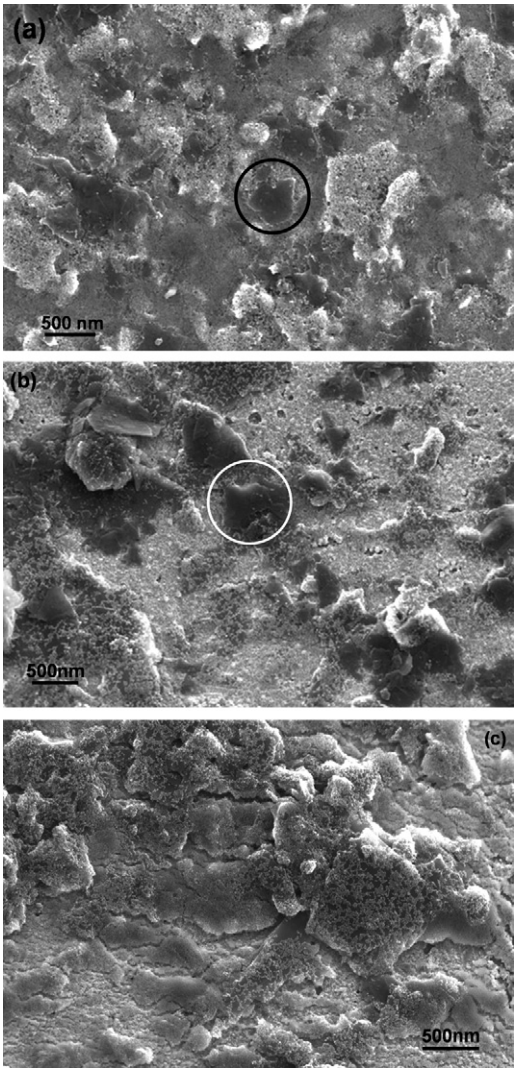

Fig. 4. SEM images at 20–25k× of the nanoparticle coating surfaces after three process cycles during (a) cLBL assembly, (b) dLBL assembly, and (c) sLBL assembly. The circles in (a) and (b) highlight exposed graphite platelets.

crude template formation was observed and a smaller fraction of the surface is coated with graphite during sequential applications than either sLBL or cLBL assembly (Fig. 4). Coatings of comparable thickness were obtained from sLBL and cLBL assemblies, consistent random nanoparticle deposition across the entire substrate surface with each process cycle.

The composition of the coatings in Fig. 2 is given by Fig. 5, where the ratio of wt% carbon (C) to wt% silicon (Si) is plotted versus the number of application cycles for the three assembly schemes. This ratio has a value of 21.4 in the mixed suspension from which cLBL assembly occurs and is indicated by the dashed line in the figure. We note that cLBL coatings exhibit the lowest ratio, consistent with the more successful competition of silica relative to graphite for surface sites as previously observed in SEM images (Fig. 3). Enhanced graphite adsorption (i.e., clustering) onto the bare gold substrate in the presence of the cationic polyacrylamide layer causes the ratio for both cLBL and sLBL assemblies to decline with additional cycles. The dLBL assembly scheme yields the highest and most persistent ratio, consistent with a more ordered alignment of graphite clusters throughout the entire coating thickness as observed in Fig. 4(c).

Coating surface morphology was also investigated using atomic force microscopy (AFM). Fig. 6 contains root mean square (rms) roughness data obtained from 20 μm × 20 μm areas of a coating

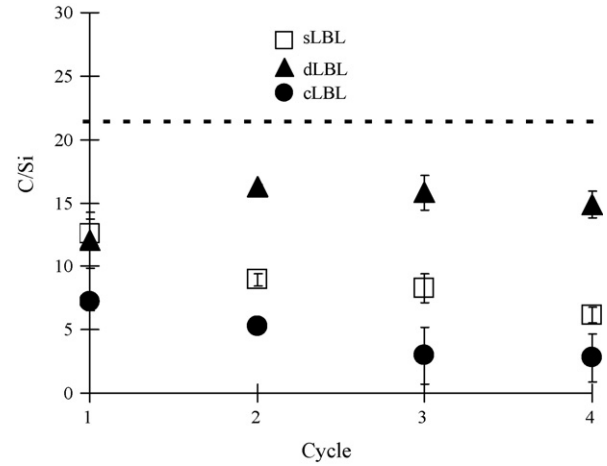

Fig. 5. Carbon to silicon wt% ratio from EDS measurements for various LBL assembled coatings. The dashed line in the figure represents the composition of the mixed nanoparticle suspension.

prepared from the three different assembly schemes. The results for eight bilayer (polyelectrolyte–nanoparticle) coatings prepared from pure graphite suspensions and pure silica suspensions are also shown in the figure by the solid and dashed lines, respectively. We note that the surface roughness of the cLBL assembled coatings is intermediate between the two pure coatings and that a plateau is approached after the application of about three cycles (as indicated by the solid line obtained from a second order fit to the data in Fig. 6). This number of cycles is comparable to that where the coating composition equilibrates (Fig. 5) and the substrate surface in nearly completely covered by graphite platelets (Fig. 4(a)). The rms roughness dependence on number of cycles for dLBL assembly is nearly identical to that of sLBL assembly and, after the coating surface structure is fully developed (three cycles), nearly identical to that of the pure graphite coating. The intermediate morphology of cLBL assembly relative to dLBL and sLBL assemblies is consistent with the higher relative silica loading of the former (Fig. 5).

3.2. *Effect of architectural LBL assembly on coating performance*

The water wetting behavior of coatings prepared utilizing either cLBL or dLBL assembly was found to be little different from that

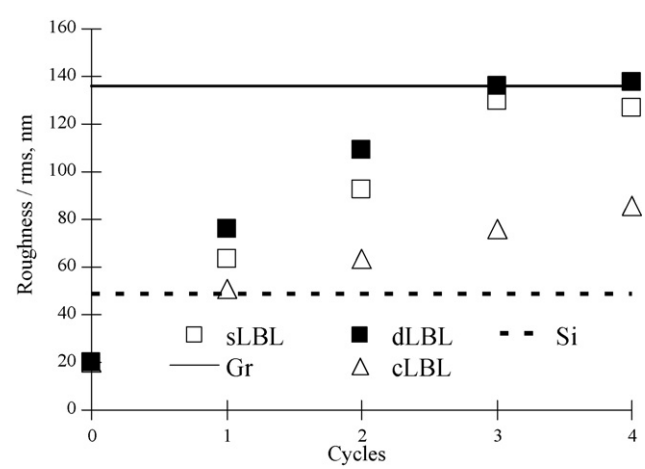

Fig. 6. AFM rms roughness obtained from 20 μm × 20 μm areas of cLBL, dLBL and sLBL assembled coatings. Data for eight polyelectrolyte–nanoparticle bilayers prepared from pure Gr and Si nanoparticle suspensions are also shown in the figure by the solid and dashed lines, respectively. The data for the pure graphite nanoparticles represent the average of that provided in Ref. [15].

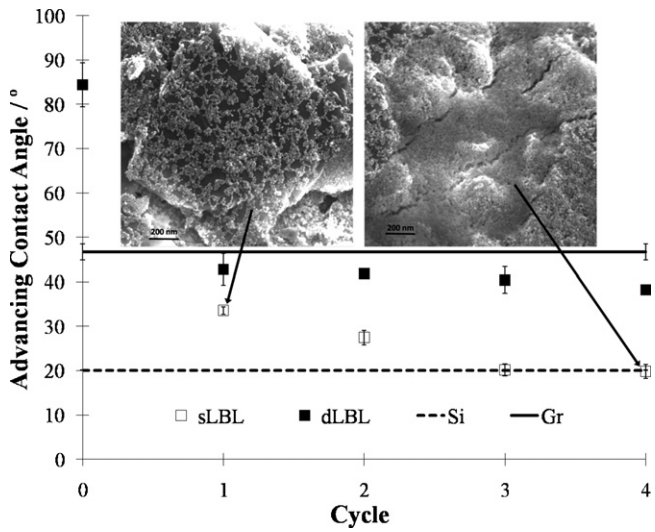

Fig. 7. Advancing contact angle data for dLBL and sLBL assembled coatings as a function of the number of process cycles. The insets are SEM images at 50k× of the surface of sLBL assembled coatings after one and four cycles, as indicated by the arrows in the figure. Data for eight polyelectrolyte–nanoparticle bilayers prepared from pure Gr and Si nanoparticle suspensions using the same process conditions are also shown in the figure by the solid and dashed lines, respectively.

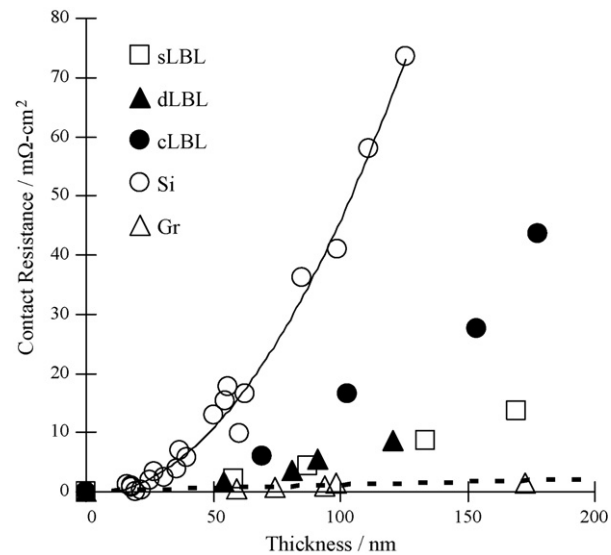

Fig. 8. Contact resistance as a function of thickness for pure nanoparticle coatings as compared to cLBL, dLBL, and sLBL assembled coatings. The data for the pure Si and Gr nanoparticles were obtained from Refs. [6,15] and are fit by solid and dashed lines, respectively.

observed with pure graphite platelets, despite the presence of a substantial amount of silica on their surface (Figs. 4 and 5). For example, after three cycles, the advancing water contact angle for either a cLBL or dLBL assembled coating was 40° compared to 84° for the bare substrate surface and 47° for a pure graphite platelet coating prepared under similar conditions, with a standard deviation less than 5° in every case. The receding contact angle was found to be ∼18° with standard deviation ∼5° in every case. Johnson and Dettre [10–12] have previously predicted that a surface composed of heterogeneous domain areas larger than molecular scale has advancing and receding contact angles that are indicative of the most hydrophobic and the most hydrophilic domains, respectively. That is, for sufficiently large surface domains, dynamic macroscopic wetting behavior is predicted to be relatively insensitive to surface chemical composition except for surfaces that are nearly homogeneous with respect to one domain or the other.

On the other hand, the Johnson–Dettre model also predicts that as domain size decreases, surface wetting sensitivity to chemical composition increases until the behavior approaches that of the Cassie equation at molecular scales [10–12,14]. Such behavior is evident when comparing the effect on the advancing water contact angle of dLBL assembly to that of sLBL assembly as shown in Fig. 7. The solid and dashed lines in the figure depict data for eight bilayers of pure graphite and pure silica coatings, respectively. For the dLBL coatings, the advancing contact angle drops abruptly to that of pure graphite after the application of a single cycle and remains steady with additional cycles, despite the presence of substantial amounts of silica on the coating surface from the initial cycle (Fig. 4(b)). The wetting behavior of sLBL is substantially different from that of dLBL, exhibiting a gradual decline in advancing contact angle with increasing number of cycles until it becomes comparable to that of a pure silica nanoparticle coating after three cycles. Examination of the high magnification SEM inset images in Fig. 7 reveals that the surfaces of the sLBL coatings, unlike those prepared using cLBL and dLBL assemblies, contain no fully exposed graphite platelets (although exposed portions of the graphite platelets between the silica nanoparticles are clearly evident). The silica nanoparticles are observed as small white spheres resting on the graphite platelets which fill the entire field of view in these images. According to the Johnson–Dettre model, the reduction in advancing contact angle of sLBL surfaces relative to either dLBL or cLBL surfaces is a result of the reduction in the size of the heterogeneous surface domains. The gradual decline in advancing contact angle with increasing number of sLBL cycles observed in Fig. 7 is thus associated with an increase in the silica nanoparticle packing density observed in the inset images.

In addition to surface chemistry, surface morphology is known to influence wetting behavior. For example, according the well-known Wenzel model [13,27], the observed contact angle should decrease with increasing roughness if the true contact angle is less than 90°. However, we note from Fig. 7 that the surface wettability of the dLBL assembled coatings does not change with the number of application cycles despite the substantial increase in rms roughness apparent in Fig. 6. In addition, the increase in contact angle of both cLBL and dLBL assembled coatings relative to a pure silica nanoparticle coating with increased roughness is not consistent with the Wenzel prediction. Surface morphology therefore does not appear to play as great a role on wetting as surface chemical composition, at least within the range of contact angles observed in Fig. 7.

A key objective of this investigation was to control coating electrical properties simultaneous to surface wetting properties. Fig. 8 is a plot of coating contact resistance versus thickness for the three different assembly schemes. Also included in the figure are pure graphite and silica data from coatings prepared utilizing various process conditions [6,15]. The pure silica and graphite are fit by solid and dashed lines, respectively. All coating architectures exhibit a monotonic increase in contact resistance with thickness. In general, coatings prepared from mixed suspensions have contact resistances which fall between those of pure silica and pure graphite. In contrast to the cLBL assembled coatings, the contact resistances of the sLBL and dLBL assembled coatings are much closer to that of pure graphite than pure silica at the larger thicknesses. It is also interesting to note that dLBL and sLBL assemblies yield comparable contact resistance as function of thickness. This observation suggests that, at a given thickness, graphite loading is more important to platelet–platelet contact between alternating layers during LBL assembly than particle distribution (i.e., template propagation in the case of dLBL assembly). A C/Si ratio of at least 6 for coating thicknesses of up to 170 nm appears sufficient to ensure substantial reduction in contact resistance of an LBL

assembled coating to nearly that of a pure graphite platelet coating. For example, in the case of an 87-nm thick composite coating, the contact resistance may reduced from that obtained for pure silica nanoparticles (36 mΩ cm^2) to 4 mΩ cm^2 while maintaining surface hydrophilicity through incorporation of graphite platelets via sLBL assembly. This is an order of magnitude reduction in the power loss in PEM fuel cell applications. No increase in the contact resistance of the coatings is observed due to possible oxidative coupling between silica and graphite after exposure to 80 °C sulfuric acid solution at pH 5 for as long as 5000 h.

4. Conclusions

In this work, we provide a methodology by which the architectural arrangement of differing nanoparticles may be controlled so as to alter the heterogeneous domain distribution and hybrid functionality of surface-assembled thin-film structures.

LBL assembly from stable mixed graphite-silica nanoparticle suspensions (cLBL assembly) yields competitive adsorption and heterogeneous domain separation at each layer. In contrast to SAMs and LbL assemblies from mixed polyelectrolyte systems, cLBL nanoparticle assembly yields a coating composition substantially different from the suspension from which the coating was formed. The slower adsorption kinetics of the graphite nanoparticles have for the first time been shown to result in greatly reduced surface adsorption from mixed suspensions with silica relative to that obtained from pure graphite suspensions.

Electrostatic repulsion between heterogeneous nanoparticles may be used to direct the formation of distinct domains within a layer during LBL assembly from pure nanoparticle suspensions as long as polymer binder is not employed between applications of the heterogeneous nanoparticles. Such a directed LBL assembly (dLBL) scheme yields phase-separated nanoparticle structures which may be used to as templates which crudely propagate the separated phases through the thickness of a coating. Graphite loading in such structures is found more important to platelet–platelet contact and electrical conductivity between alternating layers in graphite-silica composite coatings than the detailed nanoparticle distribution. Consequently, the dLBL scheme yields coatings with lower contact resistance than cLBL assembly.

Standard LBL (sLBL) assembly of alternating graphite-silica nanoparticle layers with intervening cationic polymer binder yields both high carbon loading and mixing of graphite and silica domains. The water wetting behavior of the resultant heterogeneous domain surface distribution may be modeled using the Johnson–Dettre model of contact angle hysteresis. Surface morphology does not appear to play as great a role on wetting as surface chemical composition for the heterogeneous nanoparticle systems investigated in this study. The resultant sLBL assembled coatings optimize hybrid functionality by minimizing electrical contact resistance while simultaneously maximizing surface hydrophilicity.

Acknowledgements

Funding for this work has been provided by the General Motors Corporation and is gratefully acknowledged. One of us, MA, acknowledges support from the State of Kuwait.

References

[1] S.Y. Son, J.S. Allen, Proceedings of IMECE2005, Orlando, Florida, November 5–11, 2005.
[2] C.Y. Lee, S.Y. Lee, Exp. Therm. Fluid Sci. 32 (2008) 1716–1722.
[3] G.O. Mepsted, J.M. Moore, in: W. Vielstich, A. Lamm, H. Gasteiger (Eds.), Handbook of Fuel Cells, Wiley, New York, 2003, pp. 286–293.
[4] G. Vyas, T. Xie, T.A. Trabold, Hydrophilic fuel cell bipolar plate having a plasma induced polymerization coating, US Patent 7,622,211 (2009).
[5] A.P. Angelopoulos, S. Peters, Nanoparticle coating process for fuel cell components, US Patent Application 20,070,141,238 (2007).
[6] F. Wang, S. Peters, J. Guzda, R.H. Blunk, A.P. Angelopoulos, Langmuir 25 (2009) 4384–4392.
[7] H.A. Gasteiger, W. Gu, R. Makharia, M.F. Mathias, B. Sompalli, in: W. Vielstich, A. Lamm, H. Gasteiger (Eds.), Handbook of Fuel Cells, Wiley, New York, 2003, pp. 593–610.
[8] R.K. Iler, Plural monolayer article and process for making same, US Patent 3,485,658 (1969).
[9] P.T. Hammond, Curr. Opin. Colloid Interface Sci. 4 (2000) 430–442.
[10] R.E. Johnson, R. Dettre, in: F.M. Fowkes (Ed.), Advances in Chemistry Series 43, American Chemical Society, Washington, DC, 1964, pp. 112–135.
[11] R.E. Johnson, R. Dettre, in: F.M. Fowkes (Ed.), Advances in Chemistry Series, vol. 43, American Chemical Society, Washington, DC, 1964, pp. 136–144.
[12] R.E. Johnson, R. Dettre, J. Phys. Chem. 68 (1964) 1744–1750.
[13] L. Gao, T.J. McCarthy, Langmuir 23 (2007) 3762–3765.
[14] A.B.D. Cassie, Discuss. Faraday Soc. 3 (1948) 11.
[15] M. Alazemi, I. Dutta, F. Wang, R. Blunk, A.P. Angelopoulos, Adv. Funct. Mater. 19 (2009) 1118–1129.
[16] R.K. Iler, J. Am. Ceram. Soc. 47 (1964) 194–198.
[17] D. Lee, D. Omolade, R.E. Cohen, M.F. Rubner, Chem. Mater. 19 (2007) 1427–1433.
[18] D. Lee, X. Gemici, M.F. Rubner, R.E. Cohen, Langmuir 23 (2007) 8833–8837.
[19] A. Quinn, G.K. Such, J.F. Quinn, F. Caruso, Adv. Funct. Mater. 18 (2008) 17–26.
[20] K.L. Prime, G.M. Whitesides, Science 252 (1991) 1164–1167.
[21] A.P. Angelopoulos, L.J. Matienzo, J.B. Benziger, J. Colloid Interface Sci. 212 (1999) 419–425.
[22] C. Picart, Ph. Lavalle, P. Hubert, F.J.G. Cuisinier, G. Decher, P. Schaaf, J.C. Voegel, Langmuir 17 (2001) 7414–7424.
[23] X.G. Wang, S. Balasubramanian, L. Li, X.L. Jiang, D.J. Sandman, M.F. Rubner, J. Kumar, S.K. Tripathy, Macromol. Rapid Commun. 18 (1997) 451–459.
[24] M.T. Thompson, M.C. Berg, I.S. Tobias, J.A. Lichter, M.F. Rubner, J. Van Vliet, Biomacromolecules 7 (2006) 1990–1995.
[25] A.P. Angelopoulos, Y. Kim, Fuel 81 (2002) 2167–2171.
[26] J. Goldstein, Scanning Electron Microscopy and X-ray Microanalysis, 3rd ed., Kluwer/Springer Publishers, New York, 2003.
[27] R.N. Wenzel, Ind. Eng. Chem. 28 (1936) 988.